ISSN 1068-3356, Bulletin of the Lebedev Physics Institute, 2023, Vol. 50, Suppl. 6, pp. S715–S723. © Allerton Press, Inc., 2023.
Russian Text © The Author(s), 2023, published in Kvantovaya Elektronika, 2023, Vol. 53, No. 2, pp. 176–181.

PARTICLE ACCELERATION

Laser Wakefield Acceleration in a Plasma Channel

M. S. Dorozhkina[a,b,c], K. V. Baluev[d], D. D. Kutergin[d], I. K. Lotov[d], V. A. Minakov[a,c,*], R. I. Spitsyn[c,d], P. V. Tuev[c,d], and K. V. Lotov[c,d]

[a] *Institute of Applied Physics, Russian Academy of Sciences, Nizhny Novgorod, 603950 Russia*
[b] *Novosibirsk State Technical University, Novosibirsk, 630073 Russia*
[c] *Budker Institute of Nuclear Physics, Siberian Branch, Russian Academy of Sciences, Novosibirsk, 630090 Russia*
[d] *Novosibirsk State University, Novosibirsk, 630090 Russia*
**e-mail: V.A.Minakov@inp.nsk.su*

Received November 30, 2022; revised November 30, 2022; accepted November 30, 2022

Abstract—It is shown by numerical simulations that, if a laser pulse from the eXawatt Center for Extreme Light Studies (Sarov) is used as a driver for a laser wakefield accelerator, an electron bunch with a charge of 50 pC can be accelerated to energy of 100 GeV with an energy spread of less than 1%. To this end, it is necessary to form a plasma channel 70 m long with a characteristic radius of 200 μm and a plasma density of 3×10^{15} cm^{-3} on the axis. In a denser plasma, the acceleration rate is higher, but the acceleration length and the resulting energy are smaller. The accelerator parameters can be numerically optimized using a quasistatic model describing the laser pulse in terms of its envelope, which reduces the computation time by several orders of magnitude as compared to complete models.

Keywords: laser acceleration, plasma channel, numerical simulations, plasma acceleration

DOI: 10.3103/S1068335623180057

1. INTRODUCTION

Since the particle acceleration rate in plasma is several orders of magnitude higher than the maximum acceleration rate in conventional radio-frequency resonators, plasma acceleration methods are now being actively investigated in dozens of laboratories around the world [1–3]. To date, the maximum energy acquired by electrons in plasma (42 GeV [4]) is below the record value obtained in conventional accelerators (104.5 GeV [5]); however, the development of higher power drivers [6] will make it possible to surpass it in the nearest future and thus open ways to study new physical phenomena. In this work we estimate (and verify by numerical simulations) the energy to which an electron bunch (witness) in plasma can be accelerated, if a laser pulse obtained at the Exawatt Center for Extreme Light Studies (XCELS) [7, 8] is used as a driver forming a plasma wakefield.

2. ESTIMATION OF THE ATTAINABLE ELECTRON ENERGY

First we will estimate the plasma density at which one would expect the maximum energy acquired by electrons. We proceed from the following parameters of the designed facility [8]: laser pulse energy $Q_0 = 400$ J, laser wavelength $\lambda = 910$ nm, and maximum interaction length $L = 70$ m, which corresponds to one XCELS channel. The plasma density n, as well as the laser pulse duration τ (> 25 fs) and laser-beam radius r_0 will not be fixed yet; they will be chosen during optimization. When carrying out estimation, we assume that the dimensionless amplitude of the laser pulse is neither large nor small parameter:

$$\frac{e|\mathbf{A}|}{m_e c^2} \sim 1, \tag{1}$$

where $\mathbf{A}$ is the pulse vector potential, $e > 0$ is the elementary charge, m_e is the electron mass, and c is the speed of light. We also assume that $r_0 \sim c/\omega_p$ and the accelerating field $E_z \sim E_0$, where $\omega_p = \sqrt{4\pi n e^2/m_e}$ is the plasma frequency and $E_0 = m_e c\omega_p/e$ is the wavebreaking field. Subsequent simulations should refine the assumptions made.

If we ignore the corrections related to the geometric factors, the maximum energy W_{max} of accelerated particles is determined by the ratio of the laser frequency $\omega_0 = 2\pi c/\lambda$ to the plasma frequency ω_p. Provided that the acceleration length is limited by the laser pulse diffraction, this energy is relatively low: $W_{max} \sim m_e c^2 \omega_0/\omega_p$; if this length is limited by the pulse depletion or dephasing [1], we have

$$W_{max} \sim m_e c^2 \omega_0^2/\omega_p^2 \propto n^{-1}. \quad (2)$$

The acceleration length is

$$L_{max} \sim \frac{W_{max}}{eE_0} \sim \frac{c}{\omega_p}\frac{\omega_0^2}{\omega_p^2} \propto n^{-3/2}. \quad (3)$$

The limit (2) is applicable if the pulse diffraction is suppressed in some way, for example, by a plasma channel with a density minimum on the axis. In what follows we assume that such channel exists.

The energy content per unit length of a moderately nonlinear plasma wave is independent of the plasma density, because the energy density in this wave increases as $E_0^2 \propto n$, and the volume occupied by the wave decreases as $(c/\omega_p)^2 \propto n^{-1}$. The characteristic value of the linear energy density is [9, 10]

$$\Psi_0 = \frac{m_e c^2}{4\pi r_e} \approx 2 \text{ J/m}, \quad (4)$$

where r_e is the classical electron radius. The high laser pulse energy makes it possible to reduce the plasma density, increasing the acceleration length (3) and maximum energy (2). In this case, the ratio of the laser and plasma frequencies increases, the acceleration rate decreases (staying reasonably high), the accelerated charge increases [11], and the requirements to the accuracy of positioning the accelerated bunch in the plasma accelerating structure become less stringent (due to the increase in the c/ω_p scale). If the facility length L is simultaneously the dephasing length L_{max}, the required plasma frequency is

$$\omega_p \sim \omega_0 \left(\frac{\lambda}{2\pi L}\right)^{1/3} \sim 10^{-3}\omega_0, \quad (5)$$

which corresponds to the plasma density $n \sim 2 \times 10^{15}$ cm^{-3}, plasma skin depth $c/\omega_p \sim 100$ μm, acceleration rate $eE_0 \sim 5$ GeV/m, and maximum energy $W_{max} \sim 300$ GeV.

3. NUMERICAL SIMULATION TECHNIQUE

At a large frequency ratio ($\omega_0/\omega_p \sim 10^3$) it is especially favorable to perform numerical simulations using the quasistatic code, with laser pulse described in terms of its envelope. The envelope equation [12] increases the characteristic scales that must be resolved in time and longitudinal coordinate by a factor of ω_0/ω_p [13]; the simulation grid step can be increased and the calculation time can be decreased by the same factor. The quasistatic approximation makes it possible to increase additionally the grid step over the longitudinal coordinate in the ratio of the Rayleigh length (scale of change in the laser pulse) to the plasma wavelength, i.e., increase additionally by a factor of ω_0/ω_p. However, for correct calculation of strongly depleted laser pulses, as will be shown below, the time step must be additionally decreased by a factor of ω_0/ω_p. Thus, the quasistatic model with a laser-pulse envelope gives an acceleration six orders of magnitude higher (by a factor of ω_0^2/ω_p^2) in comparison with the simulations without simplifying assumptions, using the particle-in-cell method.

The simulations will be performed using the two-dimensional axisymmetric quasistatic code LCODE [14–16] with a laser solver [17]. Let the laser pulse be linearly polarized along the x direction and move along the z direction and the x component of its vector potential be characterized by a dimensionless complex amplitude a:

$$A_x = \frac{m_e c^2}{e}\text{Re}(a(z,\xi)e^{ik_0\xi}), \quad (6)$$

where $k_0 = 2\pi/\lambda$ and $\xi = z - ct$ is the comoving coordinate. At the beginning of the interaction

$$a = a_0 \exp\left(-\frac{r^2}{r_0^2} - \frac{(\xi - 3\sigma_z)^2}{2\sigma_z^2}\right), \quad (7)$$

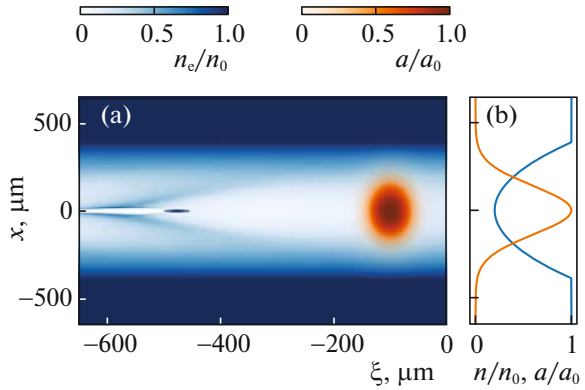

Fig. 1. Geometry of the problem: (a) the total electron density n_e in the plasma and witness and the laser pulse amplitude a at the beginning of interaction and (b) the transverse profiles of the initial plasma density n (blue curve) and laser pulse amplitude a (orange curve).

$$a_0 = \frac{2e\lambda}{\pi m_e c^2 r_0}\sqrt{\frac{Q_0}{\sigma_z\sqrt{\pi}}} \tag{8}$$

(σ_z is the pulse length). To keep the laser-beam radius constant in time, the pulse propagates in a matched plasma channel with a radial density profile

$$n(r) = \begin{cases} n_c + r^2/(\pi r_e r_0^4), & r < r_1 \\ n_c + r_1^2/(\pi r_e r_0^4), & r \geq r_1, \end{cases} \tag{9}$$

where n_c is the density on the channel axis.

Simulations show that, at $r_1 \sim 2r_0$, the beam radius pulsations in the studied range of parameters do not exceed 5%, although the channel at $r > r_1$ differs from an ideal parabolic one [1]. The density $n_0 = n(r_1)$ will be referred to as basic in the sense that it determines the value $k_p^{-1} = c/\omega_p(n_0)$, which specifies the grid steps and the computational domain radius r_{max}.

In this section we will use as an illustration the basic variant with the following set of parameters (Fig. 1): $n_c = 3 \times 10^{15}$ cm^{-3}, $\sigma_z = 34$ μm, $r_0 = 194$ μm, $r_1 = 2r_0$, and $a_0 \approx 1.4$. As will be seen further from the parametric dependencies, this variant is optimal for achieving the maximum witness energy.

While propagating through the plasma, the laser pulse loses energy, and its central frequency decreases in comparison with the initial frequency ω_0 [18, 19]. As a consequence, the function $a(\xi)$ starts oscillating with some period, which decreases as the pulse depletes (Fig. 2). To resolve these oscillations in simulations, the grid step $\Delta\xi$ must be chosen sufficiently small. In the calculations presented below, unless otherwise specified, the grid steps are $\Delta\xi = 0.0005k_p^{-1}$, $\Delta r = 0.002k_p^{-1}$, and $\Delta z = 250k_p^{-1}$; $r_{max} = 15k_p^{-1}$. At the chosen step $\Delta\xi$, there are about 50 grid nodes per laser wavelength, so that the envelope model makes it possible to increase the grid step (in comparison with the complete model) only over the z coordinate rather than over ξ. The plasma is presented as an array of macroparticles, whose weight depends on radius. There are ten macroparticles of each type (electrons and ions) per radial step Δr. Ions have a mass of $1836m_e$ (hydrogen) and can move; however, their displacement in the wave is small and does not lead to any significant physical effects. The simulation of one variant requires about 1000 CPU hours.

The correctness of simulations is verified by comparing the laser pulse energy and the energy remaining in the plasma behind the pulse. The linear energy content of plasma wave, Ψ, is calculated from the total energy flux in the moving simulation window [9, 20]:

$$\Psi = \int\left(\frac{E^2 + B^2}{8\pi} - \frac{1}{4\pi}[\mathbf{E}\times\mathbf{B}]_z\right)dS + \sum_j(\gamma_j - 1)m_j c^2, \tag{10}$$

where $\mathbf{E}$ and $\mathbf{B}$ are, respectively, the electric and magnetic fields; m_j and γ_j are, respectively, the linear mass and relativistic factor of macroparticles; integration is over the left boundary of the simulation window, and summation is over all plasma macroparticles leaving the simulation window. In the quasistatic

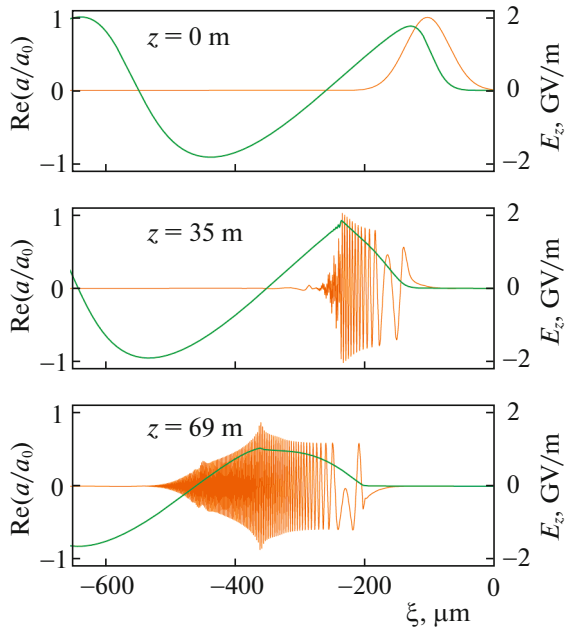

Fig. 2. Real part of the laser pulse complex amplitude Re $a(\xi)$ (orange curves) and the longitudinal electric field E_z (green curves) on the axis at different instants.

description, plasma macroparticles are considered to be not groups of real particles but "jets" of particles entering the moving simulation window on a given radius; therefore, formula (10) contains the linear macroparticle mass (mass per unit length of the "jet"). Integrating over the path passed, we find the energy left in the plasma:

$$Q_\mathrm{p}(z) = \int_0^z \Psi(z')dz'. \tag{11}$$

The laser pulse energy is obtained by integrating over the entire simulation window,

$$Q_\mathrm{l} = \int \frac{E^2 + B^2}{8\pi} dV \approx \frac{m_\mathrm{e}^2 c^4}{4\pi e^2} \int \left(\frac{\partial \,\mathrm{Re}(a e^{\mathrm{i}k_0\xi})}{\partial \xi} \right)^2 dV, \tag{12}$$

where the radial derivatives of the vector potential were neglected [21] in view of their smallness. It follows from the energy conservation law that

$$Q_\mathrm{p} = Q_0 - Q_\mathrm{l} \equiv \Delta Q_\mathrm{l}. \tag{13}$$

The accuracy with which equality (13) is fulfilled characterizes the correctness of both the laser and plasma solvers. The smaller the step $\Delta\xi$, the larger pulse propagation path can be simulated with acceptable accuracy (Fig. 3). A comparison of the plots of the energy balance and electric field, similar to those in Figs. 2 and 3 but calculated to a larger length z at different pulse parameters, also demonstrate that a laser pulse can transfer no more than 30–40% of its energy to the plasma, after which it is elongated so that ceases to excite efficiently a wakefield.

During propagation, a laser pulse, as well as the wave excited by it, shift backwards in the simulation window, which moves with a speed of light (Fig. 2). The accelerating field profile also changes. Therefore, the point of the wave at which electrons must be injected to obtain maximum energy is not obvious beforehand. To determine the coordinate ξ of the optimal injection point, we will estimate the electron energy W_est from the field integral on the axis [6]:

$$W_\mathrm{est}(\xi, z) = -e\int_0^z E_z(\xi, z')dz' + W_0, \tag{14}$$

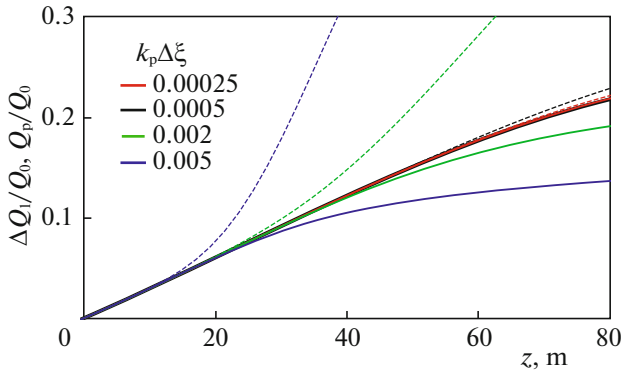

Fig. 3. Change in the laser pulse energy ΔQ_1 (dotted curves) and the total energy Q_p transferred by a laser pulse to the plasma (solid line), depending on the distance z passed in the plasma in simulations with different longitudinal grid steps $\Delta\xi$.

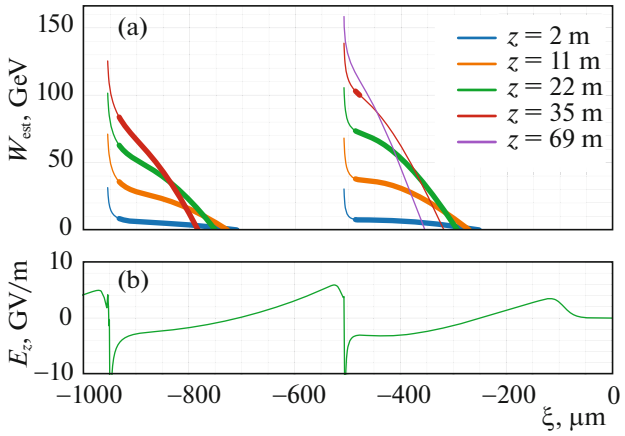

Fig. 4. (a) Estimated energy W_{est} acquired by an electron on different acceleration lengths z, depending on the electron injection coordinate ξ and (b) the electric field on the axis, E_z, at the beginning of interaction for the variant with $r_0 =$ 146 μm. Thin lines show the electron energy disregarded in estimation of the maximum energy because of their proximity to the bubble edge or residence in the laser pulse region.

excluding electrons from consideration when they find themselves in the defocusing phase of the wave or when their energy decreases to zero. The initial energy $W_0 = 300$ MeV is sufficiently high to consider that electrons do not change the coordinate x_i during acceleration. Indeed, at a constant acceleration rate eE_z, the longitudinal electron displacement $\delta\xi$ can be related to the electron relativistic factor $\gamma(z)$:

$$k_p\delta\xi \approx \int_0^{L/c} \frac{cdt}{2\gamma^2(z)} = \frac{m_e c^2 k_p}{2eE_z}\int_{\gamma(0)}^{\gamma(L)} \frac{d\gamma}{\gamma^2} = \frac{m_e c^2 k_p}{2eE_z}\left(\frac{1}{\gamma(0)} - \frac{1}{\gamma(L)}\right) \approx \frac{m_e c^2 k_p}{2eE_z\gamma(0)} \sim 0.01. \quad (15)$$

The set of the dependences $W_{est}(\xi)$ at different z values has a characteristic "triangular" shape (Fig. 4) with a maximum at the end. Electrons "survive" only in those regions where they were accelerated and focused from the very start. The electron acceleration in the second period of the wave does not lead to a much higher energy than in the first period, even if the longitudinal dependence of plasma density $n_e(z)$ is specially chosen so as to provide conditions under which the maximum accelerating field in the second period is always achieved at the same value of ξ.

Under certain conditions, when the beam radius and pulse length are smaller than in the basic variant or when the plasma density is higher, a bubble, i.e., a region free of electrons, is formed in the plasma. This is exactly the case (at $r_0 = 146$ μm) shown in Fig. 4. The field in the end of the bubble has a narrow singularity, which formally leads to acceleration of electrons to high energies. In reality, when the problem is not ideally axisymmetric, the singularity does not arise. Therefore, not to hinder the optimization as a

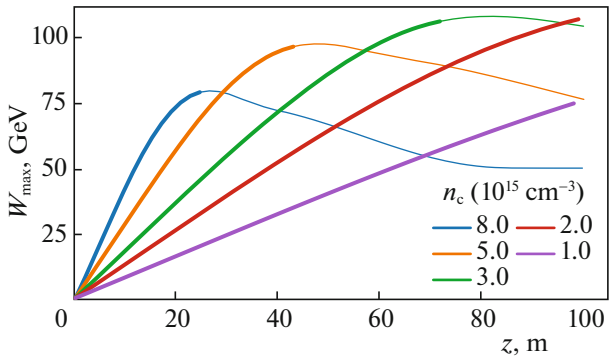

Fig. 5. Maximum energy of accelerated electrons W_{max} (estimate (14)) as a function of the acceleration length at different plasma densities on the axis (n_c). The other parameters are basic: $\sigma_z = 34$ μm, $r_0 = 194$ μm, and $r_1 = 2r_0$. Thin lines show the maximum energy with allowance for the electrons to fall in the laser pulse region.

result of its presence in the simulations, we will exclude from consideration the electrons located at a distance from the bubble end smaller than $0.5k_p^{-1}$. The bubble end is determined from the condition $E_z = 0$ on the axis. These electrons are shown by thin lines in Fig. 4.

If the trailing edge of the laser pulse starts overlapping the witness, the quality of the latter is deteriorated, because the accelerated electrons obtain an additional transverse momentum from the laser field. Therefore, the electrons that turn out to be in the laser pulse region will be disregarded during optimization. In Fig. 4 they are also shown by thin lines.

4. PARAMETRIC DEPENDENCIES

As the target function for optimization we will use the maximum energy acquired by an electron at a length $L \le 70$ m, according to estimate (14), provided that this electron is not at the end of the bubble and does not overlap with the laser pulse. To begin with, we consider the factors determining the optimal plasma density on the axis. Figure 5 presents a typical density dependence. At a low plasma density the acceleration rate is low, and the electron energy does not have enough time to reach the maximum at the length of 70 m. At a high density the laser pulse becomes rapidly depleted and elongated, due to which almost simultaneously the wave structure changes (electrons find themselves in the retarding field, and their energy ceases to rise) and the trailing edge reaches the highest energy electrons. The maximum energy decreases with an increase in the plasma density. The optimum is at $n_c \sim 3 \times 10^{15}$ cm^{-3}.

With a change in the laser pulse length one can observe the same extreme situations (Fig. 6). A long pulse provides a too low acceleration rate, whereas a short pulse becomes too rapidly depleted. In the basic variant the pulse length $\sigma_z = 34$ μm corresponds to its duration $\tau = 200$ fs, which is eight times longer than the designed minimum XCELS pulse duration. Thus, the plasma wakefield acceleration does not require any extreme compression of laser pulse in the longitudinal direction.

The dependence of the maximum energy on the beam radius does not have a clear optimum (Fig. 6): the narrower the beam, the higher the electron energy is. However, according to formula (9), a deep plasma channel is required to hold a narrow beam, in which the density plasma should change several times on the beam radius. It is fairly difficult to create such a channel. As can be seen in Fig. 6, a decrease in the beam radius to less than 200 μm does not lead to a proportionally large increase in the electron energy; therefore, the radius $r_0 \approx 200$ μm was chosen as optimal. We should also note that, if the condition $k_p r_0 \gg 1$ begins to be fulfilled with an increase in the radius r_0 or plasma density n_c, pulse filamentation is observed.

It is noteworthy that, at a small beam radius ($r_0 = 146$ μm), the electron energy barely decreases with a decrease in the plasma density n_c to zero (Fig. 6). The reason is as follows: because of the narrowness of the channel and steepness of its walls, the wakefield wavelength and the electric field in it are determined by the channel wall density rather than the plasma density on the axis. Thus, an analog of the wakefield acceleration in a hollow channel is obtained [22–24].

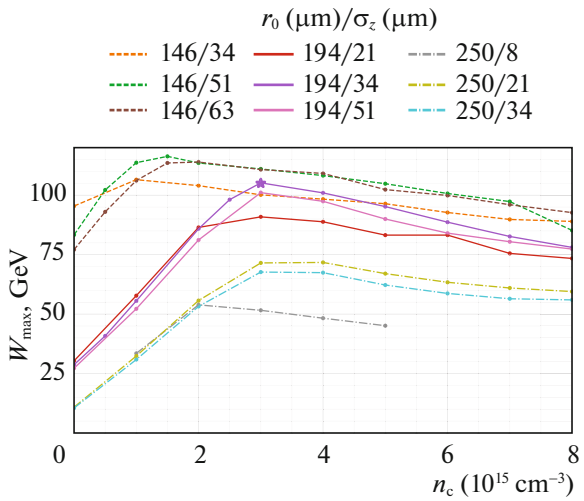

Fig. 6. Maximum energy of accelerated electrons, W_{max} (estimate (14)) as a function of the plasma density on the axis, n_c, at different values of the radius r_0 and length σ_z. The basic variant is indicated by an asterisk.

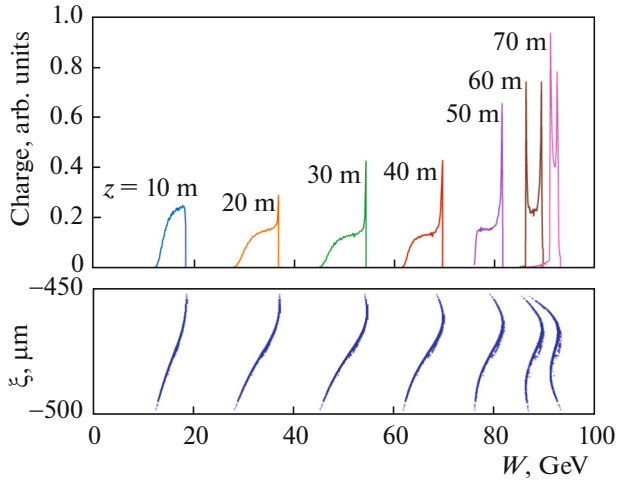

Fig. 7. Energy spectrum (top) and phase portrait (bottom) of an optimally accelerated witness with a charge of 50 pC at different distances z passed in the plasma.

5. ELECTRON ACCELERATION

The plasma wave excited in the optimal mode has an energetics sufficient to accelerate a witness with a charge of 50 pC to 100 GeV. To obtain this acceleration in simulations, one should choose the witness length σ_w and initial position ξ_0 so as to make the influence of the witness on the wave to decrease its energy spread. The optimization problem is not rigorously defined in this case, because one must choose between the increase in the average energy and the decrease in the energy spread. Nevertheless, one can reach simultaneously an average energy of 91 GeV and a relative rms spread in energy of 0.7% (Fig. 7). The position of this witness in the wave at the beginning of interaction is shown in Fig. 1. The initial witness parameters are as follows: energy 300 MeV, rms length σ_w = 10 μm, normalized emittance 2 mm mrad, and radius 2.25 μm. Since the witness has a high density and its significant part is located in the its own bubble (see Fig. 1), the initial witness radius is matched to the focusing force of the ion background. The leading edge of the witness is mismatched in this case, due to which the normalized emittance of the witness increases on the whole by a factor of 1.5 at the beginning of acceleration and does not change furthermore.

6. DISCUSSION OF THE RESULTS AND CONCLUSION

According to the numerical simulation results, the witness energy turned out to be three times lower than that expected from the estimates given in Section 2. There are two reasons for this. First, the estimate (2) [1, 25, 26] was obtained from the group velocity and rate of pulse energy loss at the beginning of interaction. In reality, the maximum energy is lower because of the synergy of depletion and dephasing. On the one hand, when the pulse central frequency decreases because of the energy loss, the group velocity decreases as well, the pulse more rapidly shifts backward in the simulation window (Fig. 2), and the dephasing length decreases. On the other hand, because of the difference in the frequencies in different parts of the pulse, the latter is elongated (Fig. 2) and ceases to excite efficiently a wave long before transferring its energy to the plasma (Fig. 3).

Second, the suggestion that a wave with a characteristic radial scale $c/\omega_p(n_c)$, where the plasma frequency $\omega_p(n_c)$ is determined by the plasma density n_c on the axis, can be excited in a matched channel turned out to be invalid. As follows from condition (9), the plasma density at $r = r_0 = c/\omega_p(n_c)$ is $5n_c$. This means that the wakefield wavelength length is determined by some density $n_{eff} > n_c$ averaged over the beam radius. The same density value determines the scale and other characteristics of the wave: frequency $\omega_p(n_{eff})$ and wavebreaking field E_0. The beam radius always turns out to be larger than $c/\omega_p(n_{eff})$, the wave energy is distributed over a region wider than $c/\omega_p(n_{eff})$, and the acceleration rate in the wave is below eE_0. This is exactly what we see in the basic variant, for which $r_0 = 2c/\omega_p(n_c)$ and $|E_z| \approx E_0/3$.

The modern techniques of injecting plasma electrons into a wakefield make it possible to obtain high-quality witnesses with an energy of 100 MeV or higher, but require precise controlling of plasma density profile [27–31] and good reproducibility of laser pulse parameters [32, 33]. The tuning of a plasma injector may require a large number of "shots" and will be impossible if pulses follow with a period of several hours and the price of one "shot" is high. Therefore, to implement a plasma injector preaccelerator, it is necessary to have a separate laser system with a high repetition frequency, as well as a flexible system for controlling the plasma profile in the injector.

The key element of the proposed acceleration scheme will be a plasma channel having no analogs in the world. In the basic variant, the channel with a twofold change in density on a scale of 200 μm should provide a laser pulse transport by 500 Rayleigh lengths. Apparently, to design such a channel, one should combine several existing techniques: capillary discharge [34–38], staging [39, 40], additional heating by an auxiliary laser pulse [41–43], and ablation of material from renewable channel walls [44]. Since the required plasma density in the channel (3×10^{15} cm^{-3}) is unusually low for the laser wakefield acceleration, one can affect the channel formation with a longitudinal magnetic field by magnetizing the transverse motion of electrons and thus suppressing the transverse thermal conductivity of the plasma [45]. At electron energy of 10 eV or less, which is characteristic of plasma heating by an auxiliary laser [43], the required channel radius (200 μm) is comparable with the Larmor radius of electrons in a magnetic field of 500 G, which can easily be implemented. Due to the large (by the standards of the laser wakefield acceleration) channel width and expected high accuracy of laser pulse control [7], the problem of inaccurate pulse focusing [46] appears to be less hazardous than in other experiments with pulse channeling.

ACKNOWLEDGMENTS

The calculations were partially performed on the computational cluster "Academician V.M. Matrosov" [47].

FUNDING

This study was supported by a scientific program of the National Center for Physics and Mathematics.

CONFLICT OF INTEREST

The authors declare that they have no conflicts of interest.

REFERENCES

1. Esarey, E., Schroeder, C.B., and Leemans, W.P., *Rev. Mod. Phys.,* 2009, vol. 81, p. 1229.
2. Joshi, C., Corde, S., and Mori, W.B., *Phys. Plasmas,* 2020, vol. 27, p. 070602.
3. Albert, F., et al., *New J. Phys.,* 2021, vol. 23, p. 031101.
4. Blumenfeld, I. et al., *Nature,* 2007, vol. 445, p. 741.

5. Workman, R.L. et al. (Particle Data Group), *Prog. Theor. Exp. Phys.,* 2022, vol. 2022, p. 083C01.
6. Lotov, K.V. and Tuev, P.V., *Plasma Phys. Controlled Fusion,* 2021, vol. 63, p. 125027.
7. Shaykin, A., Kostyukov, I., Sergeev, A., and Khazanov, E., *Rev. Laser Eng.,* 2014, vol. 42, p. 141.
8. XCELS. https://xcels.ipfran.ru/.
9. Lotov, K.V., *Phys. Rev. E,* 2004, vol. 69, p. 046405.
10. Zgadzaj, R. et al., *Nat. Commun.,* 2020, vol. 11, p. 4753.
11. Katsouleas, T., Wilks, S., Chen, P., Dawson, J.M., and Su, J.J., *Part. Accel.,* 1987, vol. 22, p. 81.
12. Mora, P. and Antonsen, T.M., *Phys. Plasmas,* 1997, vol. 4, p. 217.
13. Tuev, P.V., Spitsyn, R.I., and Lotov, K.V., *Plasma Phys. Rep.,* 2023, vol. 49, p. 229.
14. Lotov, K.V*., Phys. Rev. Spec. Top. Accel. Beams,* 2003, vol. 6, p. 061301.
15. Sosedkin, A.P. and Lotov, K.V., *Nucl. Instrum. Methods Phys. Res., Sect. A,* 2016, vol. 829, p. 350.
16. lcode. https://lcode.info/.
17. Spitsyn, R.I., *Master's Dissertation,* Novosibirsk: Novosibirsk Gos. Univ., 2016.
18. Bulanov, S.V., Inovenkov, I.N., Kirsanov, V.I., Naumova, N.M., and Sakharov, A.S., *Phys. Fluids B,* 1992, vol. 4, p. 1935.
19. Shadwick, B.A., Schroeder, C.B., and Esarey, E., *Phys. Plasmas,* 2009, vol. 16, p. 056704.
20. Spitsyn, R.I., Timofeev, I.V., Sosedkin, A.P., and Lotov, K.V., *Phys. Plasmas,* 2018, vol. 25, p. 103103.
21. Terzani, D., Benedetti, C., Schroeder, C.B., and Esarey, E., *Phys. Plasmas,* 2021, vol. 28, p. 063105.
22. Schroeder, C.B., Esarey, E., Benedetti, C., and Leemans, W.P., *Phys. Plasmas,* 2013, vol. 20, p. 080701.
23. Pukhov, A., Jansen, O., Tueckmantel, T., Thomas, J., and Kostyukov, I.Yu., *Phys. Rev. Lett.,* 2014, vol. 113, p. 245003.
24. Schroeder, C.B., Benedetti, C., Esarey, E., and Leemans, W.P., *Nucl. Instrum. Methods Phys. Res., Sect. A,* 2016, vol. 829, p. 113.
25. Esarey, E., Shadwick, B.A., Schroeder, C.B., and Leemans, W.P., *AIP Conf. Proc.,* 2004, vol. 737, p. 578.
26. Leemans, W., Esarey, E., Geddes, C., Schroeder, C., and Toth, C., *Philos. Trans. R. Soc. London, Ser. A,* 2006, vol. 364, p. 585.
27. Pollock, B.B. et al., *Phys. Rev. Lett.,* 2011, vol. 107, p. 045001.
28. Gonsalves, A.J. et al., *Nat. Phys.,* 2011, vol. 7, p. 862.
29. Wang, W.T. et al., *Phys. Rev. Lett.,* 2016, vol. 117, p. 124801.
30. Qin, Z. et al., *Phys. Plasmas,* 2018, vol. 25, p. 023106.
31. Jalas, S., Kirchen, M., Messner, P., Winkler, P., Hübner, L., Dirkwinkel, J., Schnepp, M., Lehe, R., and Maier, A.R., *Phys. Rev. Lett.,* 2021, vol. 126, p. 104801.
32. Wu, F. et al., *Opt. Laser Technol.,* 2020, vol. 131, p. 106453.
33. Maier, A.R. et al., *Phys. Rev. X,* 2020, vol. 10, p. 031039.
34. Spence, D.J., Butler, A., Hooker, S.M., *J. Opt. Soc. Am. B,* 2003, vol. 20, p. 138.
35. Jang, D.G., Kim, M.S., Nam, I.H., Uhm, H.S., and Suk, H., *Appl. Phys. Lett.,* 2011, vol. 99, p. 141502.
36. Qin, Z. et al., *Phys. Plasmas,* 2018, vol. 25, p. 043117.
37. Gonsalves, A.J. et al., *J. Appl. Phys.,* 2016, vol. 119, p. 033302.
38. Turner, M. et al., *High Power Laser Sci. Eng.,* 2021, vol. 9, p. e17.
39. Sprangle, P., Hafizi, B., Penano, J.R., Hubbard, R.F., Ting, A., Moore, C.I., Gordon, D.F., Zigler, A., Kaganovich, D., and Antonsen, T.M., Jr., *Phys. Rev. E,* 2001, vol. 63, p. 056405.
40. Qin, Z. et al., *Phys. Plasmas,* 2018, vol. 25, p. 073102.
41. Gonsalves, A.J. et al., *Phys. Plasmas,* 2020, vol. 27, p. 053102.
42. Pieronek, C.V. et al., *Phys. Plasmas,* 2020, vol. 27, p. 093101.
43. Bagdasarov, G.A. et al., *Phys. Plasmas,* 2021, vol. 28, p. 053104.
44. Swanson, K.K. et al., *Phys. Rev. Spec. Top. Accel. Beams,* 2021, vol. 24, p. 091301.
45. Froula, D.H., Divol, L., Davis, P., Palastro, J.P., Michel, P., Leurent, V., Glenzer, S.H., Pollock, B.B., and Tynan, G., *Plasma Phys. Controlled Fusion,* 2009, vol. 51, p. 024009.
46. Veisman, M.E., Kuznetsov, S.V., Andreev, N.E., *Quantum Electron.,* 2017, vol. 47, p. 199.
47. Irkutsk Supercomputer Center SB RAS. http://hpc.icc.ru. Accessed August 22, 2022.

Translated by Yu. Sin'kov